Super-resolution in digital holography by a two-dimensional dynamic phase grating

M. Paturzo[1], F. Merola[1,3], S. Grilli[1], S. De Nicola[2], A. Finizio[2], and P. Ferraro[1]

[1]CNR- Istituto Nazionale di Ottica Applicata, via Campi Flegrei 34, 80078-Pozzuoli (NA), Italy
[2]CNR-Istituto di Cibernetica, via Campi Flegrei 34, 80078-Pozzuoli (NA), Italy
[3]Dipartimento di Fisica, Università di Napoli, via Cintia, I-80126 Napoli, Italy
melania.paturzo@inoa.it, pietro.ferraro@inoa.it

Abstract: An approach that uses an electro-optically tunable two dimensional phase grating to enhance the resolution in digital holographic microscopy is proposed. We show that, by means of a flexible hexagonal phase grating, it is possible to increase the numerical aperture of the imaging system, thus improving the spatial resolution of the images in two dimensions. The augment of the numerical aperture of the optical system is obtained by recording spatially multiplexed digital holograms. The grating tuneability allows one to adjust the intensity among the spatially multiplexed holograms maximizing the grating diffraction efficiency. Furthermore we demonstrate that the flexibility of the numerical reconstruction allows one to use selectively the diffraction orders carrying useful information for increasing the spatial resolution. The proposed approach can improve the capabilities of digital holography in three-dimensional imaging and microscopy.

OCIS codes: (090.0090) Holography : Holography; (090.1760) Holography : Computer holography; (100.6640) Image processing : Super-resolution; (110.0180) Imaging systems : Microscopy; (070.6020) Fourier optics and signal processing : Continuous optical signal processing; (050.1950) Diffraction gratings.

References and links

1. B. Kemper and G. von Bally, "Digital holographic microscopy for live cell applications and technical inspection," Appl. Opt. **47**, A52-A61 (2008)
2. B. Rappaz, F. Charrière, C. Depeursinge, P. J. Magistretti, and P. Marquet, "Simultaneous cell morphometry and refractive index measurement with dual-wavelength digital holographic microscopy and dye-enhanced dispersion of perfusion medium," Opt. Lett. **33**, 744-746 (2008)
3. P. Ferraro, D. Alferi, S. De Nicola, L. De Petrocellis, A. Finizio, and G. Pierattini, "Quantitative phase-contrast microscopy by a lateral shear approach to digital holographic image reconstruction," Opt. Lett. **31**, 1405-1407 (2006)
4. W. M. Ash III and M. K. Kim, "A Demonstration of Total Internal Reflection Holographic Microscopy for the Study of Cellular Motion," in Digital Holography and Three-Dimensional Imaging, OSA Technical Digest (CD) (Optical Society of America, 2008), paper DTuB6.
5. L. Xu, X. Peng, J. Miao, and A. K. Asundi, "Studies of Digital Microscopic Holography with Applications to Microstructure Testing," Appl. Opt. **40**, 5046-5051 (2001)
6. P. Ferraro, S. Grilli, D. Alfieri, S. De Nicola, A. Finizio, G. Pierattini, B. Javidi, G. Coppola, and V. Striano, "Extended focused image in microscopy by digital Holography," Opt. Express **13**, 6738-6749 (2005)
7. F. Dubois, N. Callens, C. Yourassowsky, M. Hoyos, P. Kurowski, and O. Monnom, "Digital holographic microscopy with reduced spatial coherence for three-dimensional particle flow analysis," Appl. Opt. **45**, 864-871 (2006)
8. J. Garcia-Sucerquia, W. Xu, S. K. Jericho, P. Klages, M. H. Jericho, and H. J. Kreuzer, "Digital in-line holographic microscopy," Appl. Opt. **45**, 836-850 (2006)
9. Y. Park, G. Popescu, K. Badizadegan, R. R. Dasari, and M. S. Feld, "Fresnel particle tracing in three dimensions using diffraction phase microscopy," Opt. Lett. **32**, 811-813 (2007)
10. L. Repetto, E. Piano, and C. Pontiggia, "Lensless digital holographic microscope with light-emitting diode illumination," Opt. Lett. **29**, 1132-1134 (2004)
11. P. Picart, J. Leval, D. Mounier, and S. Gougeon, "Time-averaged digital holography," Opt. Lett. **28**, 1900-1902 (2003)

12. N. Demoli and I. Demoli, "Dynamic modal characterization of musical instruments using digital holography," Opt. Express **13**, 4812-4817 (2005) http://www.opticsinfobase.org/abstract.cfm?URI=oe-13-13-4812
13. S. De Nicola, P. Ferraro, S. Grilli, L. Miccio, R. Meucci, P. K. Buah-Bassuahc, and F. T. Arecchi, "Infrared digital reflective-holographic 3D shape measurements," Opt. Commun. **281**, 1445-1449 (2008).
14. N. George, K. Khare, and W. Chi, "Infrared holography using a microbolometer array," Appl. Opt. **47**, A7-A12 (2008)
15. L. Repetto, R. Chittofrati, E. Piano and C. Pontiggia, "Infrared lensless holographic microscope with a vidicon camera for inspection of metallic evaporations on silicon wafers" Opt. Commun. **251**, 44-50 (2005)
16. G. Pedrini, F. Zhang, and W. Osten, "Digital holographic microscopy in the deep (193 nm) ultraviolet," Appl. Opt. **46**, 7829-7835 (2007)
17. J. H. Massig, "Digital off-axis holography with a synthetic aperture," Opt. Lett. **27**, 2179–2181 (2002).
18. Sergey A. Alexandrov, Timothy R. Hillman, Thomas Gutzler, and David D. Sampson, "Synthetic Aperture Fourier Holographic Optical Microscopy," Phys. Rev. Lett. **97**, 168102 (2006)
19. Y. Kuznetsova, A. Neumann, and S. R. Brueck, "Imaging interferometric microscopy–approaching the linear systems limits of optical resolution," Opt. Express **15**, 6651-6663 (2007) http://www.opticsinfobase.org/abstract.cfm?URI=oe-15-11-6651
20. Vicente Mico, Zeev Zalevsky, Pascuala García-Martínez, and Javier García, "Superresolved imaging in digital holography by superposition of tilted wavefronts, " Appl. Opt. **45**, 822-828 (2006)
21. L. Martínez-León and B. Javidi, "Synthetic aperture single-exposure on-axis digital holography," Opt. Express **16**, 161-169 (2008) http://www.opticsinfobase.org/abstract.cfm?URI=oe-16-1-161
22. F. Le Clerc, M. Gross, and L. Collot , "Synthetic-aperture experiment in the visible with on-axis digital heterodyne holography," Opt. Lett. **26**, 1550-1552 (2001)
23. Renaud Binet, Joseph Colineau, and Jean-Claude Lehureau, "Short-Range Synthetic Aperture Imaging at 633 nm by Digital Holography," Appl. Opt. **41**, 4775-4782 (2002)
24. C. Liu, Z. Liu, F. Bo, Y. Wang, and J. Zhu, "Super-resolution digital holographic imaging method," Appl. Phys. Lett. **81**, 3143 (2002).
25. S. Grilli, M. Paturzo, L. Miccio and P. Ferraro, "In situ investigation of periodic poling in congruent LiNbO3 by quantitative interference microscopy," Measurement and Science Technology, (in press) (June 2008)
26. M. Paturzo, P. De Natale, S. De Nicola, P. Ferraro, S. Mailis, R. W. Eason, G. Coppola, M. Iodice, and M. Gioffré, "Tunable two-dimensional hexagonal phase array in domain-engineered Z-cut lithium niobate crystal," Opt. Lett. **31**, 3164-3166 (2006)
27. M. Paturzo, S. Grilli, S. Mailis, G. Coppola, M. Iodice, M. Gioffré and P. Ferraro, "Flexible coherent diffraction lithography by tunable phase arrays in lithium niobate crystals," Opt. Commun. **281**, 1950-1953 (2008)
28. F. Zhang and I.Yamaguchi, L. P. Yaroslavsky, "Algorithm for reconstruction of digital holograms with adjustable magnification," Opt. Lett. **29**, 1668-1670 (2004).
29. F. Zhang, G. Pedrini, and W.Osten, " Reconstruction algorithm for high-numerical-aperture holograms with diffraction-limited resolution," Opt. Lett. **31**, 1633-1635 (2006).

1. Introduction

Digital Holography (DH) and other similar interferometric approaches provide coherent imaging in microscopy for a variety of applications such as Quantitative Phase Microscopy in biology [1-4], characterization of silicon MEMS, three dimensional (3D) imaging [5, 6], particle image analysis [7-10], and vibration analysis [11,12]. The potential applications of DH have been extended to a wide spectral range, from far IR [13-15] to deep UV [16]. The computational image reconstruction from a digital hologram has many advantages compared to the traditional optical holography, including amplitude and phase imaging, 3D imaging and the digital wavefront manipulation. On the other hand, some disadvantages also exist. In fact, no electronic device is able to compete with the high resolution (up to 5000 lines/mm) of the photographic emulsions used in optical holography. Therefore, in most cases, the resolution achieved in DH is too low and not qualified for practical applications.

Recently, important results have been achieved for increasing the optical resolution in DH imaging, thus opening new possibilities in 3D microscopy. It is well known that, in microscopy, the resolution of the optical systems is limited by the numerical aperture (NA). Essentially, because of the finite aperture of the imaging system, only the low frequency parts of the object spectrum are transmitted and then recorded by the sensor. Therefore, the corresponding reconstructed images are band limited in the frequency domain.

Several strategies have been defined and different approaches have been tested to increase the NA of the optical system in order to get super-resolution. Most of the aforementioned methods are essentially aimed at increasing synthetically the NA of the light sensor to get super-resolution. Massig et al. increased the NA by recording nine holograms with a camera (CCD array) translated to different positions and by recombining them in a single synthetic digital hologram [17]. Alexandrov et al. were able to break the diffraction limit by rotating the sample and recording a digital hologram for each position in order to capture the diffraction field along different directions [18]. A different approach was proposed by Kuznetsova et al. who rotated the sample in respect to the optical axis in order to re-direct the rays scattered at wider angles into the aperture of the optical system, thus going beyond its diffraction limit [19]. Mico et al. proposed and demonstrated a method for enhancing the resolution of the aperture limited imaging systems based on the use of tilted illumination and common-path interferometric recording [20]. Martínez et al. translated the camera by a few microns in order to increase both the spatial resolution and the sampling in the recoding process [21]. Synthetic-aperture was gained with on-axis digital heterodyne holography by LeClerc et al. [22] while a combination of aperture synthesis and phase-shifting DH was developed by Binet et al.[23].

Recently, Liu et al. demonstrated that super-resolved images can be obtained simply by using the diffraction effect of an appropriate grating [24]. Essentially, their technique allows one to collect parts of the spectrum diffracted by the object, which otherwise would fall outside the CCD array. This was achieved by inserting a diffraction grating in the recording DH set-up. The basic principle is simple but effective. In fact, the diffraction grating allows one to re-direct toward the CCD array the information that otherwise would be lost. Basically, three digital holograms are recorded and spatially multiplexed onto the same CCD array. Super-resolved images can be obtained by the numerical reconstruction of those multiplexed digital holograms, by increasing three times the NA. Although the working principle has been demonstrated, it is important to highlight that some limitations wait to be overcome in the approach developed in [24]. The main limitations regard the properties of the grating they used for the recording process.

In this paper we present a novel approach where a special diffraction grating is used. It has three important characteristics that allow one to improve the optical resolution behind the limit imposed by the recording system. First, our grating has a two dimensional (2D) hexagonal geometry that allows one to obtain super-resolution in two dimensions. This is an important improvement compared to the technique in Ref. [24], where a 1D diffraction grating was used, thus enabling to increase the NA of the recording system only along one direction, namely the direction perpendicular to the lines of the diffraction grating. Second, we adopted a phase grating, instead of the amplitude one. The main drawback of the amplitude gratings is the smaller overall diffraction efficiency. In fact, only the light passing through the openings is used for imaging formation, that is only a part of the total amount of light illuminating the grating. This characteristic can turns out useful when the light gathering is critical. Third, since our phase grating, which was designed and fabricated in our laboratory, is made of an electro-optic substrate (lithium niobate) it has a tuneable diffraction efficiency. Concerning the diffraction tuneability, the phase grating allows one to adjust the relative intensities of the multiplexed holograms that, indeed, depend on the diffraction efficiency of the grating itself. We will show that such relative intensities can affect the quality of the super-resolved image obtained by the superimposition of the reconstructed holograms. The flexible phase grating, in fact, gives one the opportunity to optimize the recording process of the multiplexed holograms and, consequently, to improve the quality of the super-resolved images. In addition we will demonstrate that, thanks to the flexibility of the numerical reconstruction process, it is possible to use selectively only the diffraction orders that contribute significantly to increase the spatial resolution discarding those not carrying useful information.

2. Description of the dynamic phase grating and of the experimental set-up

The holographic set-up adopted in our experiments is shown in Fig. 1(a). The recording process was carried out by using a Fourier configuration in off-axis mode. The laser source is a He-Ne laser emitting at 632nm. The specimen is illuminated with a collimated plane laser beam, and a spherical laser beam from a pinhole is used as the reference beam. The distance between the pinhole and the CCD is the same as that between the object and the CCD, according to the Fourier holography configuration. The CCD array has (1024 × 1024) pixels with 7.6 micron pixel size.

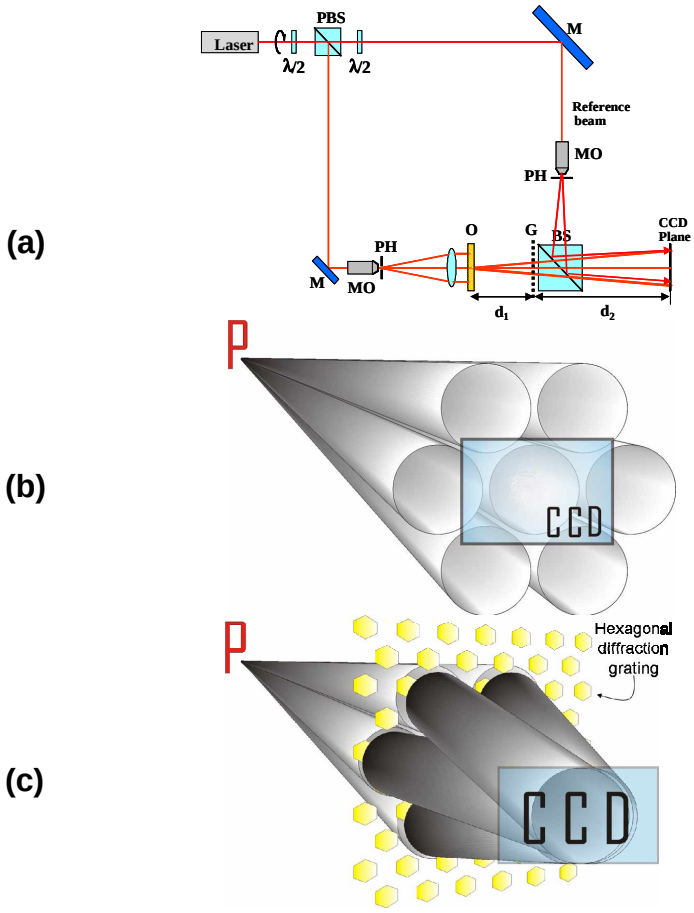

Fig. 1. (a). Scheme of the DH recording setup: Fourier configuration in off-axis mode; the ray diagrams of the object waves: (b) without the grating in the setup and (c) with the grating in the setup.

The diffraction grating G is inserted in the optical path between the object and the CCD. The diffraction grating consisted of a 2D array of hexagonally shaped periodic reversed domains in a lithium niobate (LN) substrate. The sample was prepared by standard electric field poling at room temperature and further details about the fabrication process, the working principle and the applications can be found in Refs. [25-27]. The distance between neighbouring hexagons is 35 μm. After poling, transparent ITO (indium tin oxide) electrodes were

deposited on both *z* faces of the sample in order to apply an external field across the crystal preserving the optical transmission along the *z* axis.

The phase step between opposite ferroelectric domains can be varied by changing the applied voltage across the *z*-axis of the crystal. When no voltage is applied to the crystal, no diffraction occurs since the diffraction grating is inactive (*switched-off*). When voltage is applied, the grating becomes active (*switched-on*). It is important to note that LN has a high damage threshold over a wide spectral range, from the IR to the near UV (400 nm - 5000 nm), so that the super-resolution technique presented here could be extended to wavelengths different from that used in the present work.

3. Registration of the spatially multiplexed digital holograms

As said above, because of the electro-optic effect, the hexagonal phase array appears when the voltage is applied to the LN crystal. Whenever voltage is applied, the grating becomes active (*switched-on*). It is able to generate different diffraction orders. Essentially, each diffraction order produces a corresponding digital hologram and all of the holograms are spatially multiplexed and recorded simultaneously by the CCD.

The schematic view of the object waves is shown in Figs. 1(b), 1(c) where, for sake of simplicity, only one point object P is discussed. In case of conventional holographic configurations, all of the rays scattered by the object freely propagate forward to the CCD plane, but only the central ray fan reaches the area of the hologram and can be digitally recorded, as shown in Fig. 1(b). Therefore, because of the limited aperture of the CCD array, the recorded object wave beams are only a portion of the total light scattered by the object. However, when the grating is placed between the object and the CCD array six further fan beams waves can reach the CCD. The sketch of this configuration is depicted in Fig. 1(c). Each of the six waves are produced by the first diffraction orders of the grating. The resulting digital hologram is essentially formed by seven object beams and the reference beam. In other words the CCD array simultaneously records seven digital holograms that are spatially multiplexed and coherently superimposed. The digital hologram is numerically reconstructed to obtain the in focus real image of the tested target.

The holographic system in Fig. 1(c) clearly exhibits higher NA compared to that in Fig. 1(b). In fact, the CCD aperture augments up to three times along each of the three directions at 120°, thanks to the hexagonal geometry. Consequently, the reconstructed image of the point P has a resolution enhanced up to three times compared to the usual DH system without the diffraction grating.

4. Numerical reconstruction of the spatially multiplexed digital holograms

The numerical reconstruction of the multiplexed digital hologram is divided into two steps. Firstly, the wavefield in the plane just behind the grating is obtained through the formula

$$b(x_1,y_1)=\frac{1}{i\lambda d_2}e^{\frac{i\pi}{\lambda d_2}\left(x_1^2+y_1^2\right)}\iint r(x_2,y_2)h(x_2,y_2)e^{\frac{i\pi}{d_2\lambda}\left[x_2^2+y_2^2\right]}e^{-\frac{2i\pi}{\lambda d_2}\left[x_2x_1+y_2y_1\right]}dx_2dy_2 \tag{1}$$

where $r(x_2,y_2)$ is the reference wave while $h(x_2,y_2)$ is the intensity of the digital hologram acquired by the CCD. We assume that the grating used in Fig. 2(b) has a transmission function that can be written as

$$T(x_1,y_1)=1+a\cos(2\pi x_1/p)+b\cos\left(\left(x_1+\sqrt{3}y_1\right)\pi/p\right)+c\cos\left(\left(x_1-\sqrt{3}y_1\right)\pi/p\right) \tag{2}$$

Eq. (2) is made of four terms. The first term is a constant offset. The second takes into account the diffraction along the horizontal direction, while the 3rd and 4th terms consider the two other

directions. In Eq. (2) ***p*** is the period of the grating, while **a**, **b**, and **c** are the diffraction efficiencies along the three different directions typical of the hexagonal pattern of our diffraction grating, respectively. The complex amplitude distribution of the plane immediately before the grating can be obtained by multiplying $b(x_1, y_1)$ with $T(x_1, y_1)$ and the reconstructed image in the object plane x_0, y_0 can be obtained by computing the Fresnel integral of $b(x_1, y_1)\, T(x_1, y_1)$ according to

$$b(x_0, y_0) = \frac{1}{i\lambda d_1} e^{\frac{i\pi}{\lambda d_1}\left(x_0^2 + y_0^2\right)} \iint b(x_1, y_1) T(x_1, y_1) e^{\frac{i\pi}{d_1 \lambda}\left[x_1^2 + y_1^2\right]} e^{-\frac{2i\pi}{\lambda d_1}\left[x_1 x_0 + y_1 y_0\right]} dx_1 dy_1 \quad (3)$$

We adopt the double-step reconstruction algorithm to make the reconstruction pixel (PR) in the image plane independent of the distance between the object and the CCD, differently from what occurs in a typical single-step Fresnel reconstruction process, where PR= $\lambda d/(N P_{CCD})$. In fact, in our case, the PR only depends on the ratio d_1/d_2, according to the formula PR= P_{CCD} d_1/d_2 [28]. We fix d_1 equal to d_2 so that PR= P_{CCD}=7.6 μm. In this way, we assure that the PR is the minimum achievable without decreasing the field of view, corresponding to the pixel size of the CCD.

As results by Eqs. (1) and (3), the double-step reconstruction is based on classical Fresnel algorithm. Recently, a novel method has been proposed to reconstruct high NA-holograms [29]. Nevertheless, we still adopt the classical reconstruction algorithm, since in our case the super-resolved images are obtained by superimposing a posteriori the reconstructions of spatially multiplexed holograms rather than by reconstructing a high NA-hologram.

5. Experimental results demonstrating the resolution enhancement

Figure 2(a) shows the amplitude reconstruction of the digital hologram of the object when no voltage is applied to the electro-optic grating. The object is a microscopy target with different spatial frequencies ranging from 12.59 to 100 lines/mm. The amplitude reconstruction clearly shows that the resolution is limited up to the maximum value of 31.6 lines/mm, as evidenced by the magnified view in Fig. 2(b), while pitches with 25.1 μm, 20.0 μm, 15.8 μm are clearly below the resolution limit of the system. However, as explained in the previous section, the DH system is expected to reconstruct correctly up to the extreme limit of 2×7.6 μm = 15.2 μm, according to the Nyquist criteria (at least 2 pixels per period), and taking into account that PR= 7.6 μm. Nevertheless, the reticules with pitches below 31.6 μm are clearly unresolved due to the limited NA of the system.

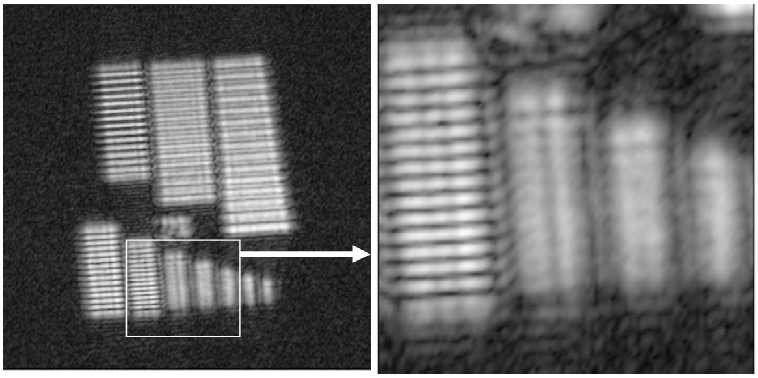

Fig. 2. (a). Amplitude reconstruction of the digital hologram when no voltage is applied to the electro-optic grating; (b) magnified view showing the reticules with the shortest pitches (31.6 μm, 25.1 μm, 20.0 μm, 15.8 μm).

When the phase grating is switched-on, seven spatially multiplexed digital holograms are recorded by the CCD array simultaneously. Figure 3 shows the amplitude reconstruction of the multiplexed digital hologram when a voltage is applied (2.5 kV in this case). The numerical reconstruction is performed by using the Eq. (3) without introducing the transmission function T(x,y) of the phase diffraction grating (see Eq. (2), i.e. T(x,y)=1).

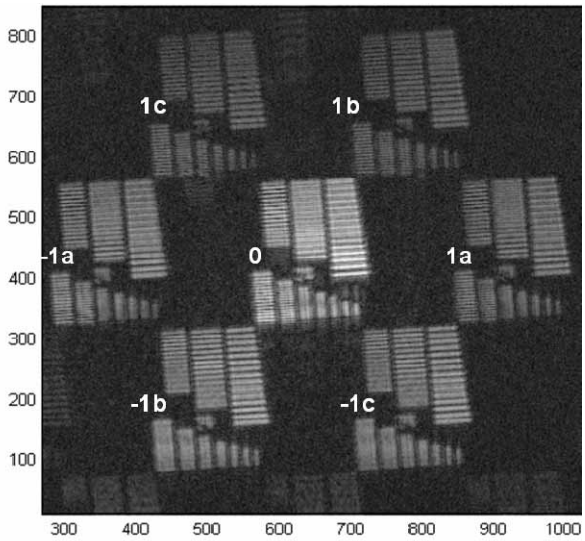

Fig. 3. Amplitude reconstruction of the multiplexed digital hologram when the phase grating is switched-on (applied voltage of 2.5 kV). This numerical reconstruction has been obtained without introducing the transmission function of the phase diffraction grating in the reconstruction algorithm (i.e. T(x,y)=1). The labels of the reconstructed images indicates the corresponding diffraction orders.

As explained before, each diffraction order produces one of the multiplexed holograms. Consequently the reconstruction process shows up seven corresponding images, one for each of the multiplexed holograms: one for the 0-th order and six for the first orders of diffraction, that are along the three typical directions of the hexagonal grating (see Fig. 3).
It can be calculated that, in order to avoid cross-talk among the various reconstructed images of the multiplexed digital hologram, the object have to be inscribable in a circle with a maximum radius of 1.3mm. This value depends on the numbers of the CCD pixels and on the pixel of reconstruction size, in our case 1024 X 1024 pixel^2 and 7.6 μm, respectively.

Each couple of images along the three different directions (encircled respectively by the yellow, blue and red ellipses in Fig. 4(a) carries different information about the object spatial frequencies spectrum. In fact, each hologram originates from the rays scattered by the object along different directions and re-directed onto the CCD area by means of the diffraction grating. It is important to point out that, without the grating (or with the grating switched-off), the information carried by the six holograms would fall outside the NA of the CCD array and would be missed.

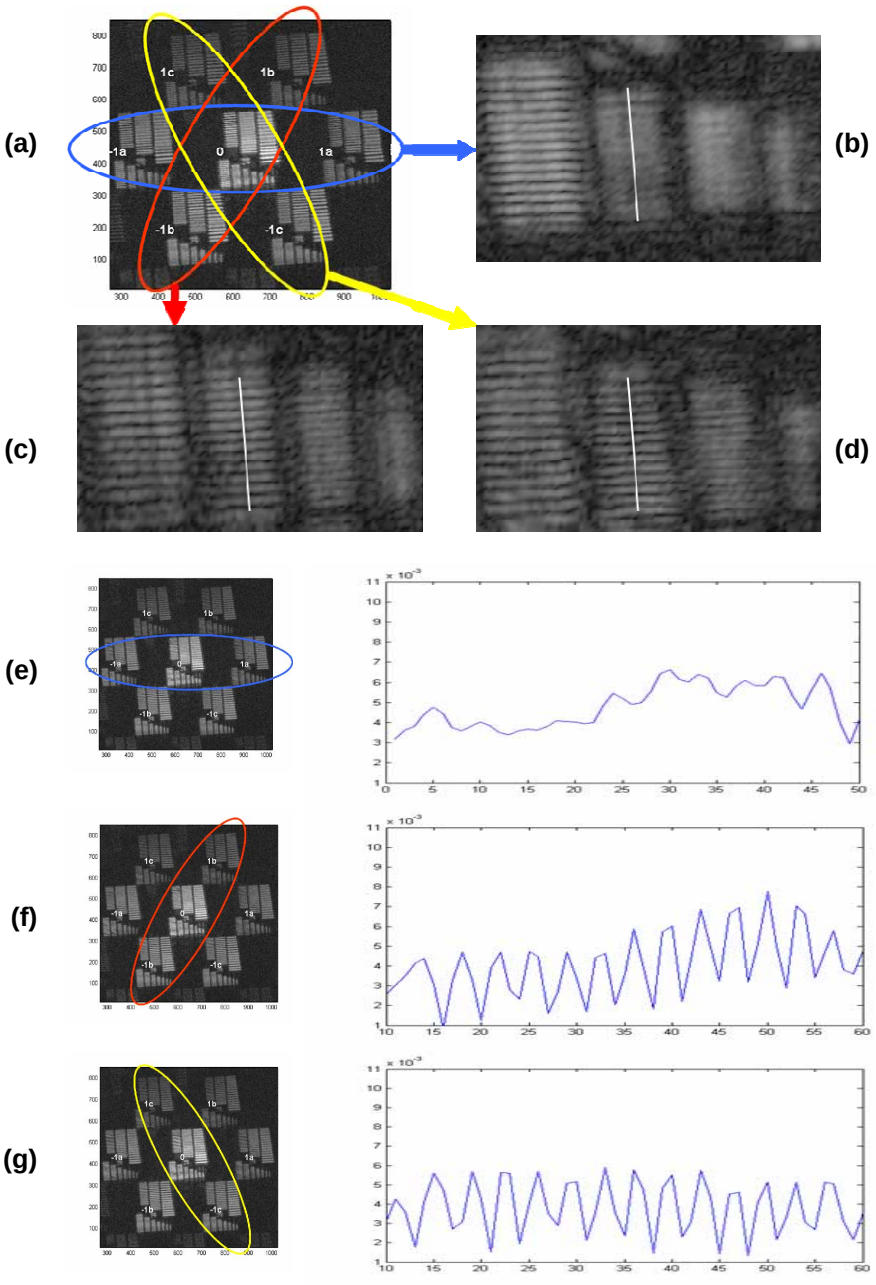

Fig. 4. (a). The coloured ellipses encircle the reconstructed images along the three typical directions of the hexagonal grating. Magnified view of the image obtained by superimposing only the -1a, 0th, +1a diffraction orders (blue ellipse in (a)); (c) the -1b, 0th, +1b orders (red ellipse); (d) the -1c, 0th, +1c orders (yellow ellipse). The reticule with a pitch of 25.1 µm, completely blurred in (b), is resolved in (c) and (d) thanks to an improvement of the optical resolution. Plot of intensity profile along the white lines in the images (b), (c) and (d) are shown in (e), (f) and (g), respectively. Axes of the plots have a.u. for intensities on ordinates while pixel number on abscissa.

The resolution enhancement can be obtained only by selectively superimposing the different reconstructed images obtained by the digital holograms. In fact, in this way, we can increase

the NA of the optical system and therefore the optical resolution of the resulting image. It is important to note that in this case we are able to get super-resolved images in 2D, differently from what was reported in ref. [24]. Even though the target used here for the imaging experiments has 1D geometry, the 2D capability of the technique is demonstrated by setting intentionally the 1D target along a direction different from the three diffraction directions of the hexagonal grating. This configuration reveals that the best image resolution can be obtained by using at least two diffraction directions, as shown by the following results. The superimposition of the reconstructed multiplexed holograms is obtained automatically by using the Eq. (3).

According to the particular geometry of the object, it is also possible to superimpose only some of the reconstructed images that effectively possess and carry the useful information with the aim at resolving the details of the object under examination. In fact, the numerical reconstruction algorithm can be considered for one, two or all of the three directions, simply assigning appropriate values to the diffraction efficiency coefficients in the Eq. (2) (i.e a, b, c, respectively).

For example, Fig. 4(b) shows the magnified view of the reconstructed image obtained by superimposing the diffraction orders **-1a**, **0th** and **+1a** (blue ellipse) only, that means we are considering just the horizontal direction. Differently, Fig. 4(c) and Fig. 4(d) show the reconstructions obtained by taking into account the **-1b**, **0th**, **+1b** and **-1c**, **0th**, **+1c** orders respectively, corresponding to the inclined directions (red and yellow ellipses). Only the last two reconstructions lead to an improvement of the optical resolution allowing one to resolve the reticule with 25.1 μm pitch, otherwise completely blurred in Fig. 4(b). This is clearly evidenced by the profiles in Figs. 4(e), 4(f), and 4(g), respectively. This result demonstrates that the collection of the rays diffracted along the horizontal direction is not useful for increasing the resolution of such target. In fact, since the rulings have only lines parallel to the horizontal direction, the rays scattered from finer rulings are directed mainly at higher angles along the vertical direction. Therefore the object frequencies have components only along the directions of the diffraction orders **±1b** and **±1c**. Consequently, in order to obtain the best signal/noise ratio in the super-resolved image, the superimposition of the orders **0th**, **±1b** and **±1c** without the **±1a** is better. Figure 5(a) shows clearly the reconstruction obtained by superimposing all of the first diffraction orders, **±1a, ±1b** and **±1c** on the zero order 0th, while Figs. 5(c) and 5(e) show the reconstructions where the **±1a** orders (corresponding to the horizontal direction) are not considered. By comparing the reconstruction in Fig. 5(a) with those in Figs. 5(c) and 5(e), it is possible to notice that, involving a useless order ($a \neq 0$) in the reconstruction, only noise is added without any benefit for the resolving power. Figures 5(b), 5(d), 5(f) show the profiles calculated along the ruling with a 25.1 μm pitch for each of the corresponding reconstructed images in Figs. 5(a), 5(c), 5(e). The super-resolved images shown in Figs. 5(c), 5(e) differ each other because they are obtained using two different sets of parameters in Eq. (2), namely (a = 0, b=2, c=4) for Figs. 5(c) and (a = 0, b=4, c=4) for Fig. 5(e).

The results show clearly that for the used object, the signal/noise ratio in the super-resolved image is increased when the two orders **±1b** and **±1c** have the same weight in the superimposition. This depends on the particular geometry of the object which has spatial frequencies all along the vertical direction, that is exactly along the bisector of the angle between the directions of the diffraction orders b and c. Therefore, the spatial frequency components along the directions of the diffraction orders **±1b** and **±1c** are the same. However, for some particular experimental conditions, the possibility to modulate the weight of each diffraction order could be useful with the aim at recovering the best super-resolved image. This selective superimposition, both in terms of selected directions and weights to be assigned to each of the considered diffraction orders, is uniquely allowed by the flexibility of such numerical reconstruction process.

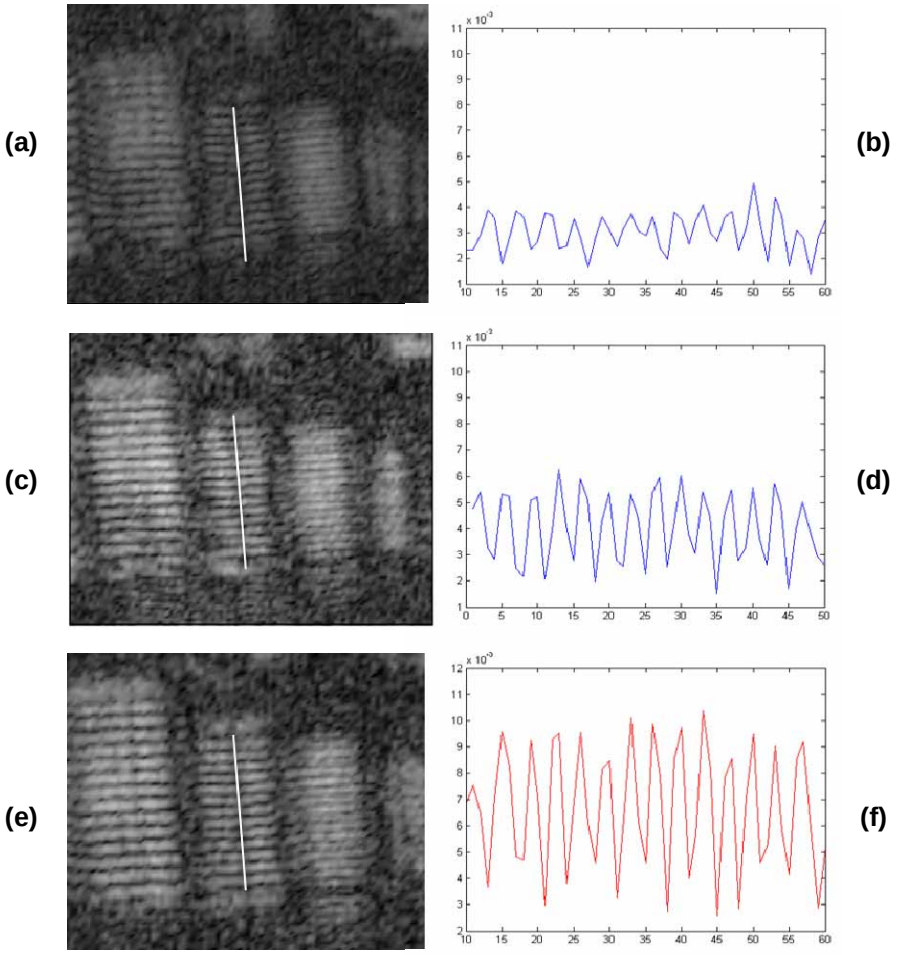

Fig. 5. (a). Amplitude reconstruction of the target obtained by superimposing all the first diffraction orders, ±1a, ±1b and ±1c, on the zero order 0th; (c), (e) amplitude reconstruction obtained by ignoring the ±1a orders and by using different or same weight for the orders ±1b, ±1c, respectively; (b), (d), (f) corresponding profiles calculated along the ruling with 25.1 μm pitch.

6. Influence of the diffraction efficiency flexibility on the super-resolved images

In addition to the analysis and optimization of the spatial resolution through the superimposition of reconstructed images relative to different diffraction orders, we have also studied how the dynamic properties of the diffraction grating can be exploited to improve the final result.

As explained above, the diffraction grating used in the experiment is an electro-optically tuneable binary phase grating. Therefore, by changing the applied voltage across the *z*-axis of the LN crystal, it is possible to tune the phase step. Consequently, the efficiency of the diffraction orders is also adjustable since it is proportional to $\sin^2(\Delta\varphi/2)$, where $\Delta\varphi$ is the

phase step between inverted domains that changes proportionally to the applied voltage V. The maximum value of the efficiency is obtained for $\Delta\varphi = \pi$ (V=2.5 kV).

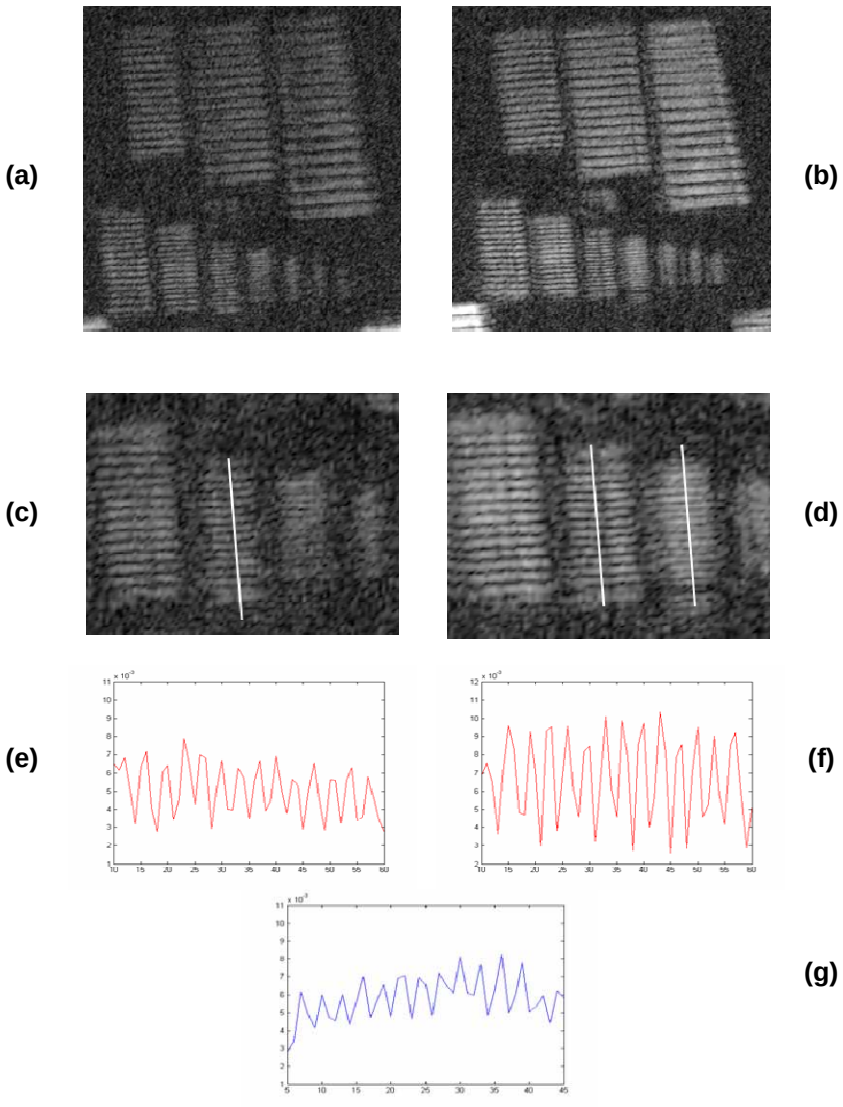

Fig. 6. (a, b). Super-resolved images optimized as to the geometrical issues, (c,d) their magnified view concerning the reticules with the shortest pitches and (e,f) the profile of the 25.1 μm pitch grating (along the white line) for $\Delta\varphi = 3\pi/5$ and $\Delta\varphi = \pi$, respectively. By Fig. 6(e), (f) it is clear that the increase of the optical resolution is higher when the phase step is $\Delta\varphi = \pi$; (g) the profile of the 20.0 μm pitch grating, clearly resolved for $\Delta\varphi = \pi$.

Figures 6(b), 6(d) and 6(f) show, respectively, the super-resolved images optimized as to the geometrical issues, its magnified view concerning the reticules with the shortest pitches and the profile of the 25.1 μm pitch grating for $\Delta\varphi = \pi$ (V=2.5 kV). Conversely, Figs. 6(a), 6(c), 6(e) show the same types of images for $\Delta\varphi = 3\pi/5$ (V=1.5 kV). The two profiles in Fig. 6(e),

(f) clearly show that the increase of the optical resolution is higher when the phase step is $\Delta\varphi = \pi$. In fact, in this case the diffraction efficiency has the maximum possible value and therefore the images coming from the diffracted orders, that contain the information about the high spatial frequencies of the object spectrum, have a high weight in the superimposition process. This is a key point, since, if the diffraction efficiency can be tuned, it is possible to find the better experimental condition for recording multiplexed digital holograms. Finally, Fig. 6(g) shows also the plot of the intensity profile for the reticule with a pitch of 20.0 μm. On the basis of this latter result we can claim an improvement of resolution at least of 1.6.

Conclusions

Super-resolution can be obtained by adopting a diffraction grating that allows one to augment the NA of the optical system. Up to now the proof of principle had been demonstrated only in the 1D case, limiting the resolution improvement to one single direction. Here we present a step forward, demonstrating that the improvement is possible in two dimensions, adopting a diffraction grating having an hexagonal geometry able to increase the NA along three different directions (i.e. the three directions typical of the hexagonal geometry). Furthermore, we add two important and novel aspects in our approach. Firstly, we adopted a dynamic phase grating obtained by electro-optic effect. The diffraction efficiency can be tuned allowing one to optimize the recording process of the digital holograms. Moreover we show that, by appropriate handling of the transmission function of the numerical grating in the reconstruction algorithm, it is possible to further improve the signal/noise ratio in the final super-resolved image.

Acknowledgments

The research leading to these results has received funding from the European Community's Seventh Framework Programme FP7/2007-2013 under grant agreement n° 216105 (“Real 3D” Project).

Authors wish to thank Mariano Gioffré of CNR-IMM Napoli for his expertise in fabricating the ITO coating for the Lithium Niobate sample.